Catalysis Today 155 (2010) 241–246

Contents lists available at ScienceDirect

Catalysis Today

journal homepage: www.elsevier.com/locate/cattod

Role of the residual Na^+ ions on the dispersion of WO_x species on titania nanotubes by in situ thermo-Raman study

M.A. Cortés-Jacome *, J.A. Toledo-Antonio, C. Angeles-Chávez, E. López-Salinas, G. Ferrat, J. Escobar, J.A. Montoya de la Fuente

Instituto Mexicano del Petróleo, Programa de Ingeniería Molecular, Eje Central Lázaro Cárdenas 152 Col. San Bartolo Atepehuacan, México, D.F., 07730, Mexico

ARTICLE INFO

Article history:
Available online 29 December 2009

Keywords:
In situ Raman spectroscopy
Titania nanotubes
Tungsten
Anatase
HRTEM
HAADF

ABSTRACT

Titania nanotubes synthesized by alkali hydrothermal method were used to support 5–20 wt.% of WO_x by wet impregnation method. Samples were characterized by in situ thermo-Raman spectroscopy, electronic microscopy and X-ray diffraction. Initially and below 400 °C, WO_x species have octahedral coordination as isolated species. After annealing at 500 °C, the nanotubular support collapsed and transformed into anatase. This event released Na^+ ions that reacted with surface WO_x species converting into sub-nanometric sodium tungstate (Na_2WO_4) particles, homogeneously dispersed on the support. At higher temperature, that is at 700 °C and 800 °C, Na_2WO_4 nanoparticles were detected on samples with W content $\leq$10 wt.%, whereas a mixture of Na_2WO_4 and $Na_2W_2O_7$ was obtained on samples with W content above 15 wt.%. A very thin layer of sodium tungstate covered the titania (anatase or rutile, depending on W loading) support after annealing at 800 °C yielding core–shell particles, with titania phase in the core and Na_2WO_4 and/or $Na_2W_2O_7$ on the shell.

1. Introduction

Tungsten oxide has been used for several catalytic applications such as alcohol dehydrogenation, n-alkanes isomerization, oxidative desulfurization, cracking and others [1,2]. WO_3 is generally dispersed on different supports such as Al_2O_3, SiO_2, ZrO_2, Nb_2O_5 and TiO_2 [2]. The high acidity, redox and photo-catalytic properties of WO_x/TiO_2 are attractive for the industrial application of these catalysts, specifically for selective catalytic reduction of NO_x by ammonia in exhaust gases, olefins conversions and oxidation reactions [3,4]. However, the industrial catalysts are prepared with commercially available TiO_2 supports, which limit the tungsten content to 10 wt.% of WO_3 for a monolayer coverage, due to the low specific surface area of the support. In order to increase the amount of WO_3 loading at the monolayer level, Eibl et al. used the oxyhydroxide precursor of titania support, obtaining two different tungstate species on the surface of TiO_2 [5]. One is a three-dimensional tungsten structure and the other one is tungsten species strongly bonded to TiO_2 support, which very likely form Ti–O–W linkages. Catalytic activity of WO_x/TiO_2 in n-pentane isomerization reaction resembles that showed by tungstated zirconia catalysts [6], and apparently there is no difference between catalysts prepared starting with a crystallized or amorphous oxyhydroxide titania support [7].

Recent developments in synthesis methods indicate that anatase or rutile phases of titania can be converted into hydrous titanates with nanotubular morphology by a relatively simple alkali hydrothermal method [8,9], exhibiting specific surface area as large as 425 m^2/g [10,11]. Nevertheless, the thermal stability of nanotubes is limited, and at temperatures above 400 °C, the nanotubular structure collapse yielding anatase nanoparticles with poor textural properties [12]. Apparently, residual Na^+ ions remaining in the interlayer space of the nanotube's walls contribute to stabilize the nanotubular structure. During the annealing treatment, the nanotubular structure collapses and transforms into anatase, expelling the residual Na ions on the surface which should be considered when dispersing transition metal oxides and/or metal on the surface titania nanotubes (TNTs) [13].

Recently we have reported the use of a hydrous titania with nanotubular morphology as an efficient support for the dispersion of a high amount of surface WO_x [14]. Initially, WO_x species remain in octahedral coordination and after the collapse of the nanotubular structure at temperatures as high as 500 °C, the TNTs release residual Na^+ ions that react with WO_x species, changing their coordination from octahedral to tetrahedral. The obtained surface sodium tungstate particles were highly active in the oxidation of dibenzothiophene [14]. Accordingly, Liu et al. have demonstrated that TNTs are able to disperse high V_2O_5 loadings (~30 wt.%) close to the monolayer dispersion with outstanding performance in the selective oxidation of methanol to dimethoxymethane [15]. In Both WO_x/TNT and V_2O_5/TNT mild reaction

* Corresponding author. Fax: +52 55 91756380.
E-mail address: macortes@imp.mx (M.A. Cortés-Jacome).

0920-5861/$ – see front matter © 2009 Elsevier B.V. All rights reserved.
doi:10.1016/j.cattod.2009.11.010

temperatures were required. However, for higher temperatures the role of the residual Na^+ ions should not be disregarded.

In this work, different WO_x loadings 5–20 wt % were homogeneously dispersed on TNTs. Structural evolution of WO_x species on the surface of TNTs was followed by in situ thermo-Raman spectroscopy in a LinKam cell at 500, 700 and 800 °C in an air flow. Additionally, samples were characterized by X-ray diffraction (XRD) and high-resolution transmission electron microscopy (HRTEM).

2. Experimental

2.1. 2.1. Preparation of WO_x/TiO_2

Titania nanotubes were synthesized by an alkali hydrothermal treatment following a procedure published elsewhere [14]. The starting support dried at 100 °C had a specific surface area of 310 m^2/g. The residual amount of Na^+ ions contained in the nanotubular support was about 2.6 wt %. Impregnation of tungsten species over hydrous nanotubular titania was achieved by an aqueous impregnation method. Twenty-two grams of the support were placed in contact with an ammonium metatungste $[(NH_4)_6H_2W_{12}O_{40}]$ solution at 6 ml/g with variable concentration in order to obtain 5, 10, 15 and 20 wt.% W loaded on the support. The pH was adjusted to 10.0 with a few drops of ammonium hydroxide. The slurry was aged 1 h at room temperature, and then excess water was eliminated at 100 °C, in a rotary evaporator. Finally, the resulting material was placed in an oven at 110 °C overnight. Throughout this study, the samples will be referred to as *x*-WNT where *x* represents W wt.% (from 0 to 20) and NT stands for titania nanotubes.

2.2. Characterization

Textural properties were determined in an ASAP-2000 analyzer from Micromeritics. Specific surface area (SSA) was calculated from N_2 physisorption at 196 °C using the Brunauer–Emmet–Teller (BET) equation. Pore size distribution was obtained by the Barrett–Joyner–Halenda (BJH) method in the desorption stage. Dried samples were outgassed at 100 °C and those calcined at 500–800 °C were outgassed at 350 °C.

2.2.1. Raman spectroscopy

The Raman spectra were recorded using a Jobin Yvon Horiba (T64000) spectrometer, equipped with a confocal microscope (Olympus, BX41) with an Ar ion laser operating at 514.5 nm at a power level of 10 mW. The spectrometer is equipped with a CCD camera detector. Twenty mg of dried powdered WO_x/titania nanotubes (with different contents of tungsten 5–20 wt.%) were placed in a Linkam cell CCR1000 directly adapted to the microscope of the instrument; the cell allows the use of controlled atmosphere and temperature. The glass window of the cell was 1 mm thick. The samples were measured independently each one, heated at a 10 °C/min rate in 100 cm^3/min flowing air at indicated temperatures, and then, it was kept at this temperature for 10 min. Thereafter, the sample was cooled to room temperature and the spectra were recorded. This procedure was repeated for each temperature (500, 700 and 800 °C). An air atmosphere was used throughout all measurements.

2.2.2. X-ray diffraction

X-ray diffraction patterns was obtained by transferring a sample at the end of the in situ thermo-Raman study, that is, after annealing at 1000 °C, in a packed glass holder. The XRD analysis was recorded at room temperature with Cu K_α radiation in a Bruker Advance D-8 diffractometer having theta-theta configuration and a graphite secondary-beam monochromator. Diffraction intensity was measured in the 2θ range between 15° and 80°, with a 2θ step of 0.02° for 3 s per point.

2.2.3. High-resolution transmission electron microscopy

Transmission electron microscopy was carried out in a JEM-2200FS equipment with accelerating voltage of 200 kV. The microscope is equipped with a Schottky-type field emission gun and an ultra high-resolution (UHR) configuration (Cs = 0.5 mm; Cc 1.1 mm; point-to-point resolution, 0.19 nm) and in-column energy filter omega-type. Prior to the analysis, the samples were ground, suspended in isopropanol at room temperature and dispersed by ultrasonic agitation. Then, an aliquot of the solution was dropped on a 3 mm diameter lacey carbon copper grid. The tungsten particles in the samples were revealed by using high angle annular dark field (HAADF) detector in the scanning transmission electron microscopy (STEM) mode. STEM is particularly useful in nanoparticles studies by using a HAADF detector, which collects electrons that undergo Rutherford scattering; thus the image can be acquired where the intensity is approximately proportional to Z^2 (Z being the atomic number of the scattering atom). Therefore, elements with a high Z show higher intensities and a white contrast in the image. This technique is useful to distinguish the presence of different chemical elements, when there is a large difference in the atomic number among them, such as supported catalysts. Chemical analysis by energy dispersive X-ray spectroscopy (EDXS) was performed in a NORAN spectrometer.

3. Results and discussion

The textural properties of WO_x/NT materials are shown in Table 1. The SSA of 0-WNT support, after annealing at 400 °C, decreased from 310 to 257 m^2/g, which is a consequence of the

Table 1
Textural properties of 0–20-WNT annealed at indicated temperatures.

Sample	Annealing temperature (°C)	Specific surface area (m^2/g)	Surface density (W at./nm^2)
0-WNT	100	310	0.0
0-WNT	400	257	0.0
05-WNT	500	80	1.6
10-WNT	500	72	3.7
15-WNT	500	71	6.8
20-WNT	500	68	10.6
05-WNT	700	16	9.6
10-WNT	700	17	20.5
15-WNT	700	12	49.1
20-WNT	700	9.8	93.6
05-WNT	800	7.0	14.3
10-WNT	800	7.0	51.8
15-WNT	800	2.7	217.6
20-WNT	800	2.2	380.0

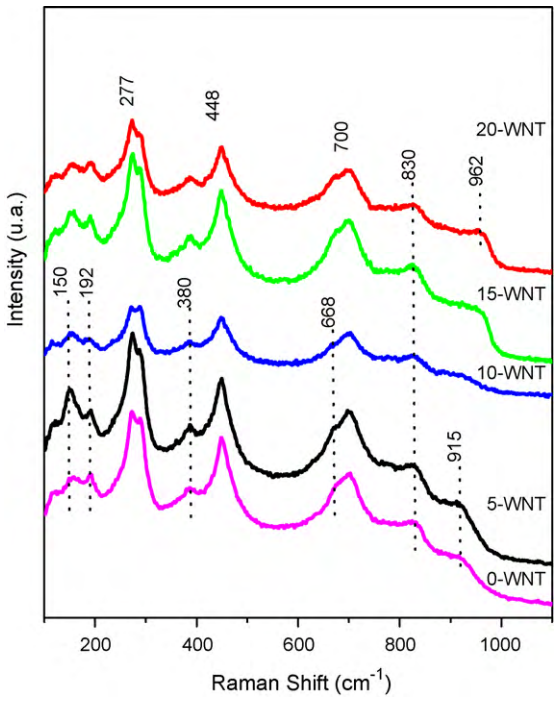

Fig. 1. Raman spectra of different WO_x loadings on titania nanotubes at 110 °C.

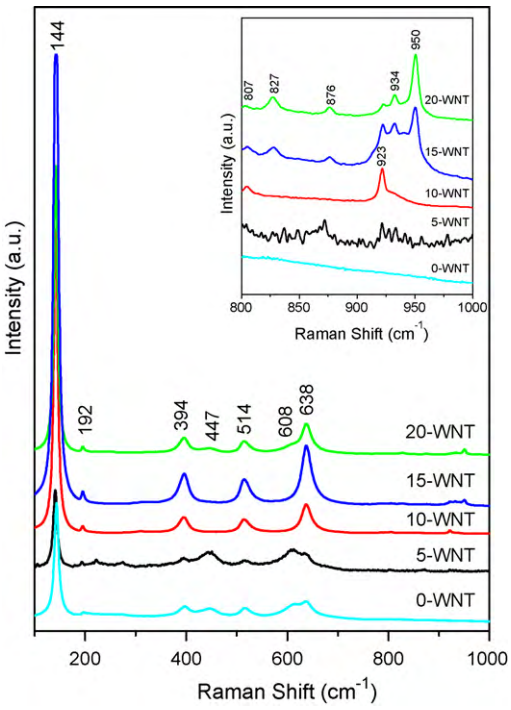

Fig. 3. Raman spectra of different WO_x loadings on titania nanotubes annealed at 700 °C. Inset: magnification of the tungstates' vibrating region.

conversion of the layered nanotubular structure into anatase domains on the walls, while maintaining the global nanotubular morphology [11]. After annealing WO_x/NT materials at 500, 700 and 800 °C, the SSA dropped considerably to ~75, 14 and 5 m^2/g respectively, and the internal porosity of nanotubes practically disappeared, producing nanoparticles or rod-like particles. The W surface density (W at./nm^2) was calculated from the SSA values and the real amount of W loaded, both values reported in Table 1.

As synthesized samples and dried at 110 °C showed Raman spectra in Fig. 1 with main vibrating bands at 277, 448 and 700 cm^{-1}. 0-WNT was included as a comparison. Other less intense bands appeared at 150, 192, 380, 668, 830 and 915 cm^{-1},

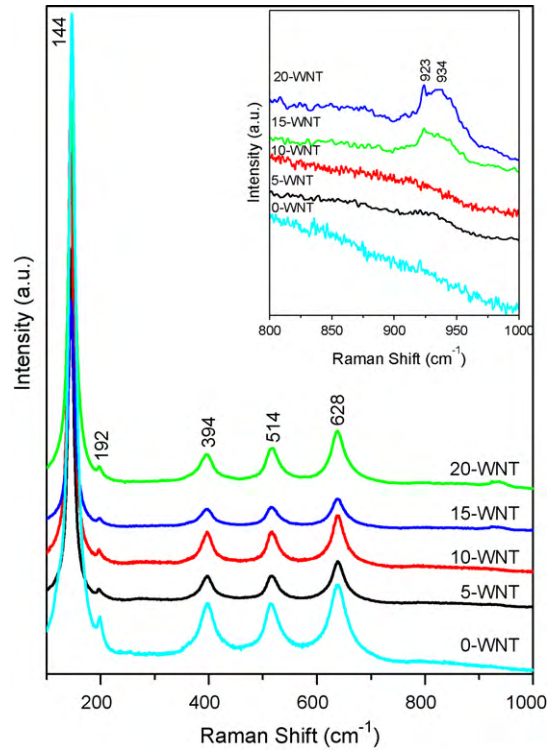

Fig. 2. Raman spectra of different WO_x loadings on titania nanotubes annealed at 500 °C. Inset: magnification of the tungstates' vibrating region.

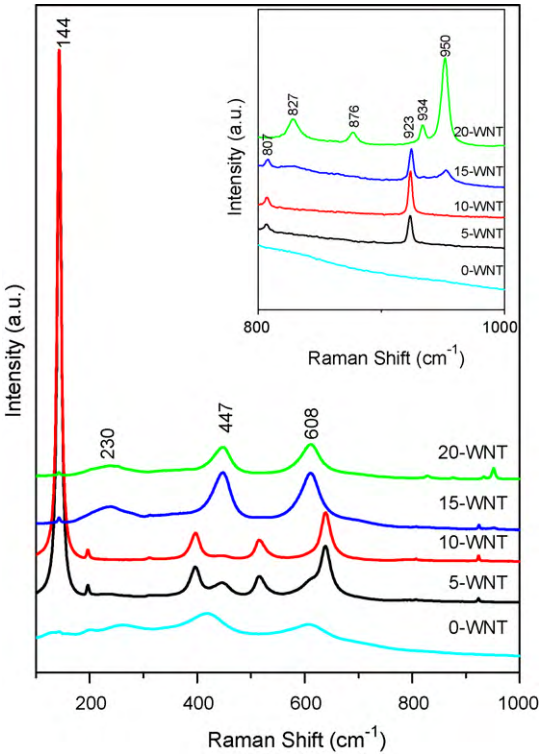

Fig. 4. Raman spectra of different WO_x loadings on titania nanotubes annealed at 800 °C. Inset: magnification of the tungstates' vibrating region.

characteristic of the nanotubular structure of hydrous titanates [16,17] as shown in Fig. 1. Only in the case of 15-WNT and 20-WNT a broad vibrating band at 962 cm^{-1}, not observable in lower W loadings, was detected. Accordingly, this band is characteristic of W=O bond in octahedral coordination and suggest the presence of highly dispersed WO_x species [18].

As can be observed in Fig. 2, for samples in situ annealed at 500 °C, the samples were predominantly made up of anatase phase showing bands at 144, 192, 394, 514 and 628 cm^{-1} [19]. Additionally, the inset in Fig. 2 shows a Raman spectra with enlarged scale in the 800–1000 cm^{-1} region which indicates that in the case of W concentration between 5 and 10 wt.% a very broad peak around 923 cm^{-1} points out the presence of Na_2WO_4 [20]. In fact in 10-WNT this band appeared smeared out probably because of heterogeneity of the sample. Several factors may influence the peak's broadness: low loading, a distorted coordination environment and/or high dispersion, among others. Inferring from and comparing with the samples of higher W concentration (e.g. 15-WNT and 20-WNT in Fig. 2), which show clear bands from a crystalline Na_2WO_4, one can say that this band arises from a Na_2WO_4, in which tetrahedrally coordinated W atoms may have differently distorted environments, so that a broad band at 923 cm^{-1} is generated, at higher temperatures (700 and 800 °C) this band will become more distinguishable and clearly associated to Na_2WO_4.

At higher W content, e.g. 15 and 20 wt.%, a narrow vibrating band at 923 cm^{-1} and a broad one at 934 cm^{-1} appeared. The first

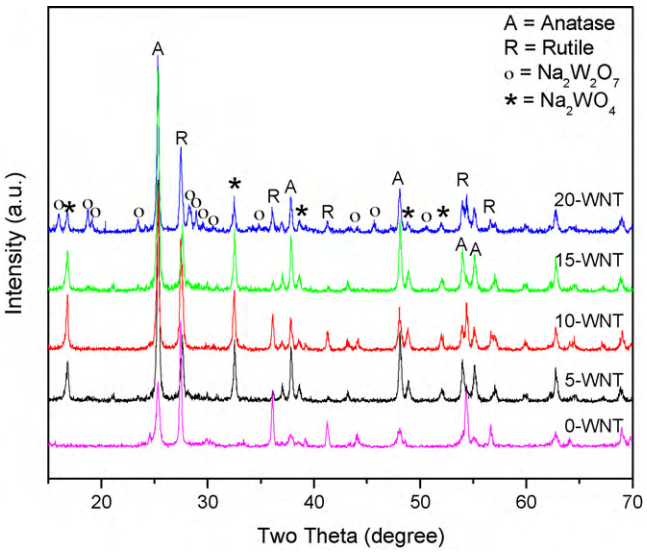

Fig. 5. XRD patterns of a WO_x/TiO_2 sample, after annealing at 700 °C.

one has been attributed to the vibration of W=O bonds in tetrahedral coordination in Na_2WO_4 phase [20]. After the nanotubular structure collapse, the material release the Na^+ ions initially confined in the interlayer space, reacting with WO_x

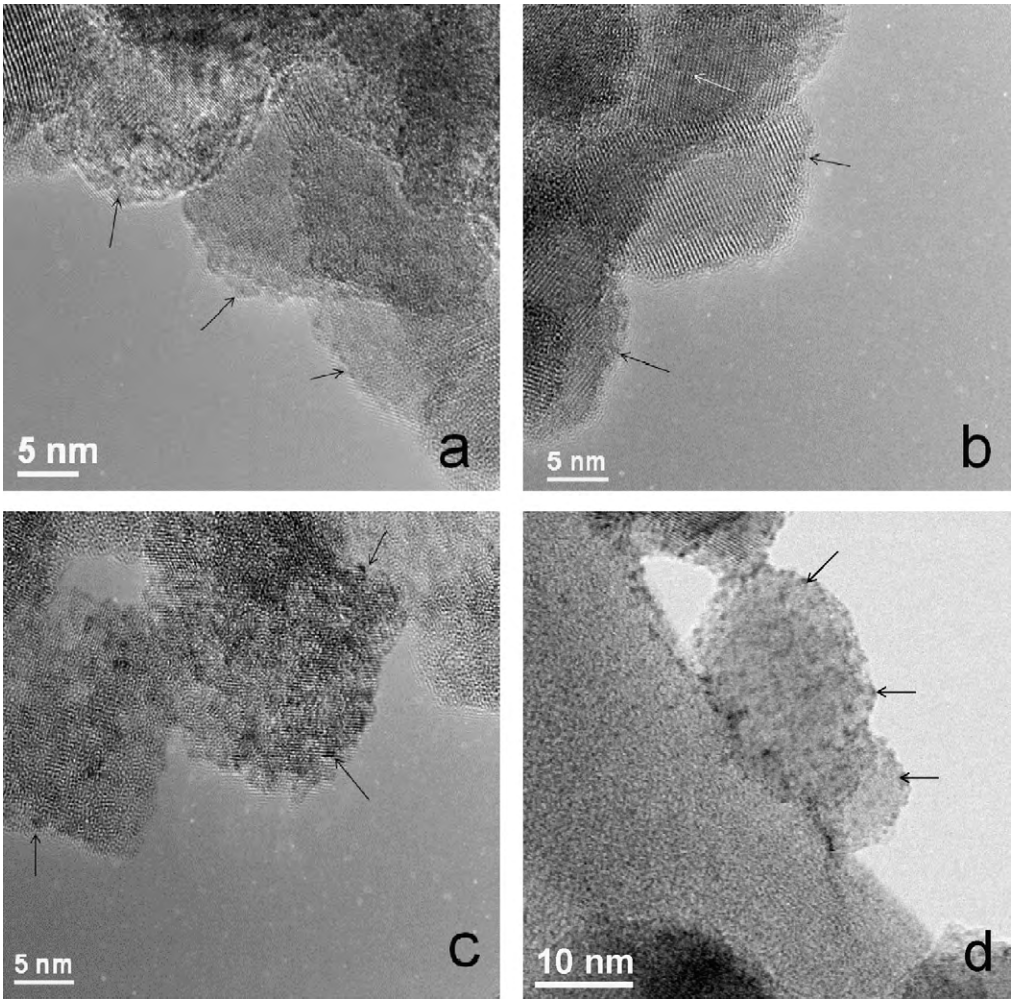

Fig. 6. HRTEM image showing Na_2WO_4 nanoparticles (see arrows in the images) on the titanium oxide support at different tungsten loadings annealed at 500 °C. (a) 5-WNT, (b) 10-WNT (c) 15-WNT and (d) 20-WNT.

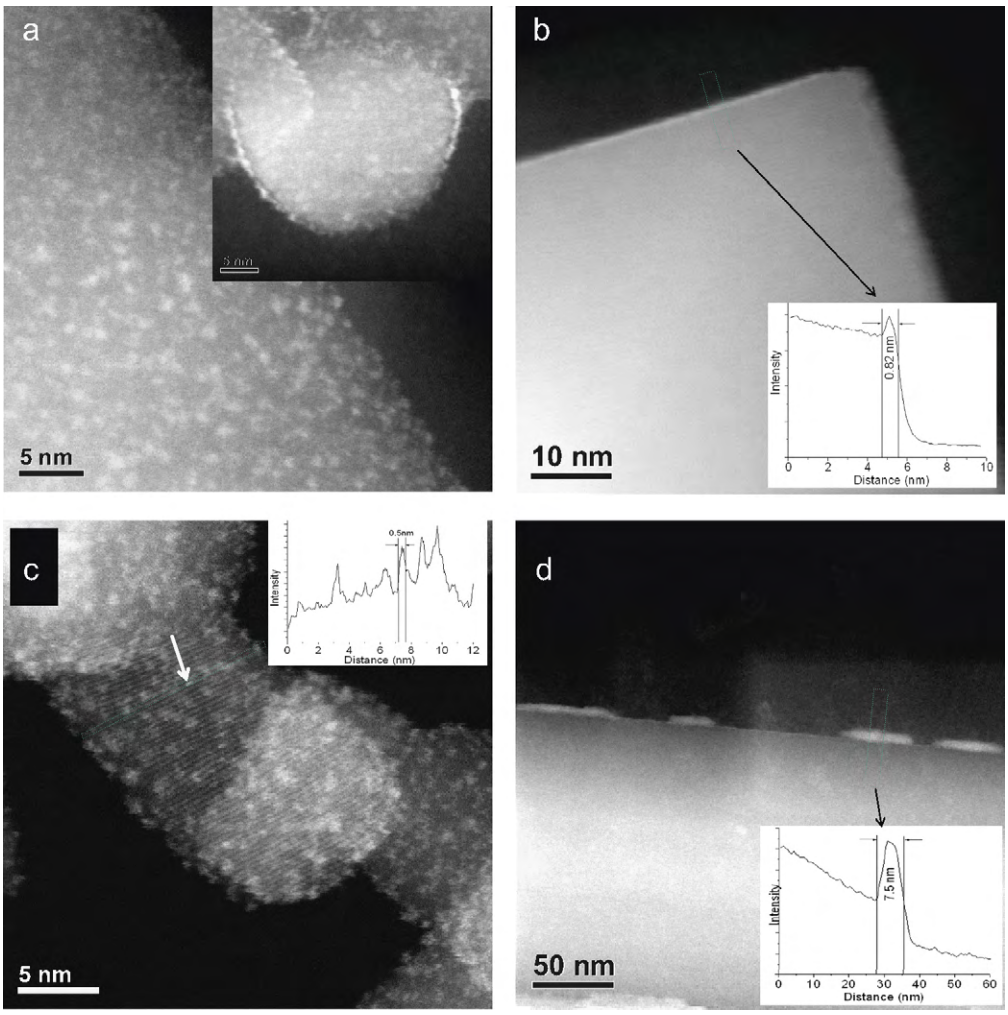

Fig. 7. Typical HAADF images of: (a) 5-WNT and (b) 5-WNT; (c) 15-WNT annealed at 700 °C and (d) 15-WNT annealed 800 °C. Insets in (b–d) are intensity profiles of indicated zones. Brighter dots represent W-rich nanoparticles.

species, yielding the Na_2WO_4 phase [14]. The accompanying broad peak at 934 cm^{-1} likely arise from isolated WO_4^{2-} tetrahedral species strongly bonded to the surface of anatase [20].

Raman spectra of samples in situ annealed at 700 °C are presented in Fig. 3. As can be noted, the structure of anatase support partially transformed into rutile, showing characteristic bands at 235, 447 and 608 cm^{-1} [21], along with those of the anatase phase. On the other hand, in the WO_x vibrating region (see inset in Fig. 3), 5-WNT and 10-WNT samples showed two bands at 923 and 934 cm^{-1}, characteristic of tetrahedrally coordinated WO_x species in Na_2WO_4 phase and WO_4^{2-} anions bonded on the surface, respectively [22], as observed on samples with high W content annealed at 500 °C (Fig. 2). Another less intense band at 807 cm^{-1} confirms the presence of Na_2WO_4 crystallites on the surface of support the [20]. At higher W content, 15-WNT and 20-WNT, in addition to the bands at 923 and 934 cm^{-1}, four sharp vibrating bands at 827, 876, 932–940 and 950 cm^{-1} were observed, being characteristic of the W=O bonds in tetrahedral and octahedral coordination of $Na_2W_2O_7$ phase [20,23], since the $Na_2W_2O_7$ structure contains both WO_4 and WO_6 units joined in infinite polymeric chains, with W atoms exhibiting both tetrahedral and octahedral oxygen coordination. The Raman bands at 950, and 932–940 cm^{-1} have been assigned to the symmetric W=O stretching mode of WO_4 units, whereas the bands at 827 and 876 cm^{-1} have been assigned to W=O stretching mode of WO_6 octahedral [20,24].

At 800 °C, the support completely transformed into rutile in samples with W content higher than 10 wt.%, as shown in Fig. 4. Then, at low W loadings rutile and anatase phases coexist. In other words, higher amounts of W induce the anatase transformation into rutile. In the case of the WO_x vibrating signals in 5-WNT and 10-WNT only sharp Raman bands at 923 and 807 cm^{-1} were observed from Na_2WO_4 phase, whereas at higher W content, 15-WNT and 20-WNT, characteristic bands of Na_2WO_4 phase at 923 and 807 cm^{-1} appear with those of $Na_2W_2O_7$ phase at 950, 934, 827 cm^{-1} (see inset in Fig. 4). In 20-WNT, the Raman spectra showed exclusively the vibrating bands characteristic of the $Na_2W_2O_7$ phase, indicating that Na_2WO_4 additionally reacted with isolated WO_x species to yield $Na_2W_2O_7$ as reported elsewhere [25].

In summary, highly dispersed WO_x species have octahedral coordination on the surface of nanotubes at 120 °C. At 500 °C, along with the partial transformation of nanotubes' surface into anatase, released Na^+ ions (from the NT) react with WO_x species yielding Na_2WO_4 phase. At higher annealing temperature, that is, at 700 and 800 °C, and 15–20 wt.% W content Na_2WO_4 react with additional WO_x species to form $Na_2W_2O_7$ phase.

X-ray diffraction patterns from the samples with different W loadings (5–20 wt.%), annealed at 700 °C, confirm the crystal phases observed by Raman spectroscopy, as shown in Fig. 5. XRD indicates that the support structure, regardless of W loading, is made up of a mixture of anatase and rutile phases. Between 5 and 15 wt.% W, some smaller peaks from the sodium tungstate phase,

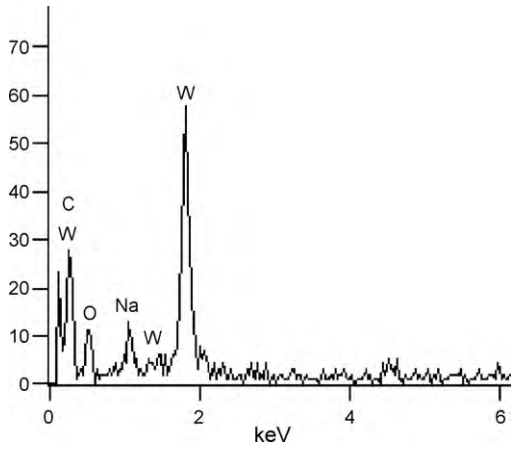

Fig. 8. EDX spectrum of the brighter dots displaying the presence of sodium in the nanoparticles.

Na_2WO_4 phase (JCPDS 11-0772), were observed. At 20 wt.% W, other intense peaks corresponding to $Na_2W_2O_7$ (JCPDS card 32-1186) appeared, along with those of Na_2WO_4. In other words, in 20-WNT, mainly $Na_2W_2O_7$ along with Na_2WO_4 coexist. Finally, in the materials annealed at 800 °C (not shown), the support was completely transformed into rutile and $Na_2W_2O_7$.

HRTEM observations carried on the samples after in situ annealed in the Linkam cell are shown in Fig. 6. In the samples annealed at 500 °C, the support's particles appear dotted by very small black entities (marked with an arrow in the Fig. 6), corresponding to Na_2WO_4 nanoparticles, as determined above by Raman and XRD. The size of these Na_2WO_4 nanoparticles is in the subnanometer scale, i.e. below 1 nm, in all examined range of W content. Only their density appears to increase along with the W content.

In order to highlight the Na_2WO_4 nanoparticles on the support, HAADF-STEM technique was used. The HAADF images display brighter contrast on heavier atoms than on lighter atoms. After annealing at 700 °C, the density the Na_2WO_4 nanoparticles increased on the surface of the support in all samples, as can be observed in Fig. 7a and c; white bright dots arise from Na_2WO_4 nanoparticles. From these observations, it is likely that 1–2 nm Na_2WO_4 nanoparticles form a thin shell around the anatase phase of the support (see Fig. 7a). At higher W content, the nanoparticles consisted of a mixture of Na_2WO_4 and $Na_2W_2O_7$ phases as observed by Raman. The high interaction between these nanoparticles with the support can be appreciated in 15-WNT, in which the atomic columns of anatase phase appeared decorated by very small brighter nanoparticles, as observed in Fig. 7c. The size of these nanoparticles was around of 0.5 nm, as indicated in the intensity profile inset in Fig. 7c.

At 800 °C, HAADF-STEM images showed a continuous thin layer (~1 nm thick, see intensity profile inset Fig. 7b) of Na_2WO_4 covering the surface of the support in 5-WNT, as shown in Fig. 7b. In contrast, the white thin layer thickness increased to 7.5 nm in 15-WNT (see intensity profile inset Fig. 7d). At this temperature, the shell layer is made up mainly of $Na_2W_2O_7$ phase. Noteworthy, some regions of the continuous layer are disrupted and separated from the support. A confirmation that the continuous layer contains Na and W atoms is given by a local chemical analysis by EDX spectrum, as shown in Fig. 8.

4. Conclusions

WO_x species were homogeneously dispersed on the surface of titania nanotubes obtained by alkali hydrothermal method. After annealing at 500 °C, the nanotubular structure of the support collapse and release interstitial Na^+ ions which react with the WO_x species yielding Na_2WO_4 characterized by a Raman band at 923 cm^{-1}. One additional Raman band is observed at 934 cm^{-1} attributed to isolated WO_4^{2-} species. At higher temperature and W content, the Na_2WO_4 phase reacts with isolated WO_4^{2-} species yielding $Na_2W_2O_7$ phase with Raman bands at 950, 934, 876 and 827 cm^{-1} arising from the symmetric vibrations of the W=O in WO_4 and WO_6 units characteristic of the structure. The bands at 950 and 934 arise from the tetrahedral WO_4 unit whereas the Raman bands at 876 and 827 cm^{-1} come from the octahedral WO_6 units.

Acknowledgement

This work was financially supported by IMP projects D.00446, and D.00447.

References

[1] M. Hino, K. Arata, J. Chem. Soc. Chem. Commun. (1987) 1259.
[2] I.E. Wachs, T. Kim, E.I. Ross, Catal. Today 116 (2006) 162.
[3] L.J. Alemany, L. Lietti, N. Ferlazzo, P. Forzatti, G. Busca, E. Giamello, F. Bregani, J. Catal. 155 (1995) 117.
[4] C. van Schalkwyk, A. Spamer, D.J. Moodley, T. Dube, J. Reynhardt, J.M. Botha, Appl. Catal. A 255 (2003) 121.
[5] S. Eibl, B.C. Gates, H. Knözinger, Langmuir 17 (2001) 107.
[6] S. Eibl, R.E. Jentoft, B.C. Gates, H. Knözinger, Phys. Chem. Phys. Chem. 2 (2000) 2565.
[7] V. Lebarbier, G. Clet, M. Houalla, J. Phys. Chem. B 110 (2006) 22608.
[8] T. Kasuga, M. Hiramatsu, A. Hoson, T. Sekino, K. Niihara, Langmuir 14 (1998) 3160.
[9] G.H. Du, Q. Chen, R.C. Che, Z.Y. Yuan, L.M. Peng, Appl. Phys. Lett. 79 (2001) 3702.
[10] C. Cheng, H. Teng, Chem. Mater. 16 (2004) 4352.
[11] J.A. Toledo-Antonio, S. Capula, M.A. Cortés-Jácome, C. Angeles-Chavez, E. López-Salinas, G. Ferrat, J. Navarrete, J. Escobar, J. Phys. Chem. C 111 (2007) 10799.
[12] D.V. Bavykin, J.M. Friedrich, A.A. Lapkin, F.C. Walsh, Chem. Mater. 18 (2006) 1124.
[13] M.A. Cortés-Jácome, C. Angeles-Chávez, M. Morales, E. López-Salinas, J.A. Toledo-Antonio, J. Solid State Chem. 180 (2007) 2682.
[14] J.A. Toledo-Antonio, M.A. Cortés-Jácome, M. Morales, C. Angeles-Chávez, L.F. Ramirez-Verduzco, E. López-Salinas, Chem. Mater. 19 (2007) 6605.
[15] J. Liu, Y. Fu, Q. Sun, J. Shen, Micropor. Mesopor. Mater. 116 (2008) 614.
[16] T. Gao, H. Fjellvåg, P. Norby, J. Phys. Chem. B 112 (2008) 9400.
[17] M.A. Cortés-Jácome, G. Ferrat-Torres, L.F. Flores Ortiz, C. Angeles-Chávez, E. López-Salinas, J. Escobar, M.L. Mosqueira, J.A. Toledo-Antonio, Catal. Today 126 (2007) 248.
[18] T. Kim, A. Burrows, C.J. Kiely, I.E. Wachs, J. Catal. 246 (2007) 370.
[19] S. Kelly, F.H. Pollak, M. Tomkiewicz, J. Phys. Chem. B 101 (1997) 2730.
[20] J.A. Horsley, I.E. Wachs, J.M. Browm, G.H. Via, F.D. Hardcastle, J. Phys. Chem. 91 (1987) 4014.
[21] H.L. Ma, J.Y. Yang, Y. Dai, Y.B. Zhang, B. Lu, G.H. Ma, Appl. Surf. Sci. 253 (2007) 7497.
[22] J.M. Stencel, Raman Spectroscopy for Catalysts, Van Nostrand Reinhold, New York, 1990, p. 85.
[23] F. Knee, R.A. Condrate, J. Phys. Chem. Solids 40 (1979) 1145.
[24] E.I. Ross-Medgaarden, I.E. Wachs, J. Phys. Chem. C 111 (2007) 15089.
[25] K. Schofield, Energy Fuel 17 (2003) 191.